Numerical Study of a Non-Linear Porous Sublimation Problem With Temperature-Dependent Thermal Conductivity and Concentration-Dependent Mass Diffusivity

Vikas Chaurasiya
Department of Mathematics,
Institute of Science,
Banaras Hindu University,
Varanasi 221005, India
e-mail: vikas.chaurasiya5@bhu.ac.in

Ankur Jain
Department of Mechanical and
Aerospace Engineering,
The University of Texas at Arlington,
Arlington, TX 76019
e-mail: jaina@uta.edu

Jitendra Singh
Department of Mathematics,
Institute of Science,
Banaras Hindu University,
Varanasi 221005, India
e-mail: jitendra.singh@bhu.ac.in

Sublimation heat transfer occurs in a wide range of engineering processes, such as accelerated freeze drying (AFD), energy storage, and food technology. Particularly in the microwave AFD process, preservation of material with the least possible energy consumption is desirable. In connection with this, it is of interest to analyze the effect of temperature/concentration dependent heat/mass transfer properties. Given the limited literature available on sublimation, there is a general lack of physical understanding of this particular problem. The present work analyzes the nonlinear sublimation process driven by convective heat/mass transfer and evaporation of water vapor using the Legendre wavelet collocation method (LWCM). Results from the present work are shown to be in excellent agreement with the exact solution of the special case of a linear problem. Further, the present numerical technique shows good agreement with finite difference method in case of a completely nonlinear model. The model is used for a comprehensive investigation of the impact of the problem parameters, on the rate of sublimation. It is found that the sublimation rate increases with increasing values of β_1 and decreasing values of β_2. The impact of other dimensionless problem parameters such as Péclet numbers Pe_1 and Pe_m, convection due to mass transfer of water vapor β, latent heat of sublimation l_0 and Luikov number Lu on sublimation process is also discussed in detail. These observations offer a comprehensive theoretical and mathematical understanding of sublimation heat/mass transfer for improving the performance and efficiency of freeze-drying and related engineering processes. [DOI: 10.1115/1.4057024]

Keywords: temperature and concentration dependent thermal conductivity and mass diffusivity, respectively, sublimation, heat and mass transfer, sublimation interface, convection, Legendre wavelet collocation method

1 Introduction

Theoretical understanding of heat and mass transfer phenomena [1] involving a moving interface is of much importance in several engineering processes such as sublimation [2,3], separation [4,5], food drying [6,7], heat/moisture migration in soils and grounds [8–11] and vacuum freeze-drying [12]. While solid–liquid phase change has been widely studied [13], sublimation is also an important, but relatively less studied phase change process. Sublimation is the process of direct conversion of a solid to vapor without passing through a liquid phase [14]. Sublimation is caused by the absorption of energy into the solid that fulfills the internal energy required for state transition, i.e., the latent heat and work done by the molecules at a fixed pressure. Sublimation occurs when the triple point pressure is so high that heating the solid results in direct vaporization even before reaching the melting point. Sublimation of solid carbon dioxide, also known as dry ice, is well-known and is commonly used. When heated at reasonable pressures, arsenic sublimes at 615 °C. Sublimation of ice is an important process in the thermodynamics of the earth [15]. Sublimation of frozen moisture in a porous body plays a key role in several engineering technologies, such as primary and secondary freeze-drying and accelerated freeze-drying (AFD) technology [16]. The sublimation process is also widely used in chemistry for purification [17]. Temperature and moisture concentration gradients drive heat and mass transfer processes in a porous body. When the temperature of the body rises above the sublimation point, it results in a sublimation front that moves with time. Similar to solid–liquid phase change problems [18,19], determination of the position of this interface is usually of primary interest. This is, in general, a nonlinear problem with analytical solutions possible only for a limited set of simple problems.

1.1 Literature Survey. In a capillary porous body, enthalpy transfer occurs in addition to the movement of the liquid, so that heat and mass transfer occur in a coupled form. Specifically, the motion of liquid may occur not only due to volumetric liquid concentration gradients but also because of the temperature field. Fick's equation and Fourier's equation have been used for describing mass transfer and heat transfer, respectively, in capillary porous bodies. Luikov [20] proposed a detailed mathematical model for heat and mass transfer in a capillary porous body, which has come to be known as the Luikov system. Cho [21] presented an exact solution describing the evaporation

Contributed by the Heat Transfer Division of ASME for publication in the Journal of Heat and Mass Transfer. Manuscript received July 14, 2022; final manuscript received February 14, 2023; published online March 20, 2023. Assoc. Editor: Igor Shevchuk.

process involving heat and mass transfer in a porous body and concluded that large latent heat resulted in delayed evaporation. Mikhailov [22] proposed two analytical mathematical formulations, related to the drying of a moist body in the period of decreasing rate and intensive drying with molar transfer in the evaporation region. It was concluded that the state of vaporization characterizes the effect of deepening of the vaporization front during transient heat and mass transfer in the porous system. Mikhailov also presented an exact solution describing the solidification of a porous body [23].

Heat and mass transfer in phase change processes can be highly coupled and complicated, especially if the solid medium is porous [20–23]. Lin [24] presented an analytical mathematical formulation for heat and mass transfer involving sublimation of a porous half-space. This model did not consider convective heat and mass transfer, and was later extended, to analyze the optimal conditions for sublimation rate in a porous half space [25]. Peng et al. presented an analytical model for the freeze-drying problem involving sublimation and desorption, in which mass transfer was controlled by Fick's law [16], or both Fick's and Darcy's laws [26]. Later, Peng and Chen [27] addressed the problem of sublimation and desorption with the addition of pressure and permeability. Recently, Jitendra et al. [28] presented an extensive analysis of the impact of convective heat transfer due to water vapor and convection during sublimation in a porous half-space. The processes of sublimation, evaporation, and freezing in a porous plate were studied experimentally and numerically by Zhang et al. [29].

Temperature-dependence of thermophysical properties may be important in the modeling of sublimation [30]. However, with nonlinear thermal properties, the treatment of problems involving heat and mass transfer is not straightforward. As a result, a number of methods have been used for such nonlinearities, including the homotopy-perturbation method [31,32], wavelet technique [33,34], similarity solution [35], and the heat-balance integral method [36].

1.2 Motivation for the Present Work. Recent papers by Jitendra et al. [28] and Lin [24] have presented analysis of heat and mass transfer during sublimation in the presence of convection and in the absence of convection, respectively. However, the convection term in the porous frozen region and the convective term related to moisture transfer of the water vapor in the vapor region were not accounted for. Convection due to mass transfer of the water vapor is particularly relevant for the vapor region [37,38], and, therefore, is the focus of the present work. Moreover, the thermal conductivity and mass diffusivity of materials are, in general, temperature- and concentration dependent, respectively. The influence of such dependence [39] is relevant to the design of practical engineering processes, and, therefore, is investigated here.

1.3 Contribution of Present Work. Based on the discussion above, key gaps in the available literature on sublimation analysis include insufficient modeling of the temperature-dependent thermal conductivity, concentration-dependent mass diffusivity, and convective term of moisture transfer caused by water vapor in the vapor region. The analysis presented in this work attempts to address these gaps. In particular, the present work accounts for temperature-dependent thermal conductivity and concentration-dependent mass diffusivity in the modeling of sublimation heat and mass transfer through the use of the Legendre wavelet collocation method (LWCM).

2 Problem Statement and Mathematical Modeling

2.1 Problem Statement. Consider the problem of sublimation of a solid material contained within the pores of a one-dimensional rigid solid porous half-space that is initially at the sublimation temperature throughout, as shown in Fig. 1. Upon sublimation, the vapor formed may diffuse or advect through the pores of the body [20–23]. The environment pressure around the body is assumed to be sufficiently small so that the pressure acting on the frozen part is dominated by the vapor pressure of the moisture. Therefore, it may be assumed that throughout the sublimation process, the vapor pressure acting on the frozen region is equal to the atmospheric pressure (which remains unchanged). Under these assumptions, sublimation will occur at a constant sublimation temperature corresponding to the vapor pressure acting on the vapor region. Several additional assumptions are also made in order to formulate the sublimation process. Vapor is considered to be an ideal gas due to its low vapor pressure. Initial concentration distribution of the wetted porous body is assumed to be uniform, denoted by C_0. For convenience, it is assumed that at the sublimation state, p_v/T_vR_0, the value of C_0 is higher than the vapor molar concentration. Here, T_v and p_v denotes the sublimation temperature and vapor pressure acting on the vapor region, respectively, and R_0 is the universal gas constant. The wetted porous body is assumed to be initially at the fixed sublimation temperature T_v. The sublimation process is assumed to be driven by a fixed molar concentration of the moisture, $C_s(< C_0)$ and a fixed temperature $T_s(> T_v)$ at $x = 0$. $s(t)$ represents the position of the sublimation front, so that the region $0 < x < s(t)$ describes the vapor region in which both heat as well as mass transfer occurs. The effect of the convective term due to the moisture flow of the water vapor is accounted for in the vapor region. Both conduction as well as convection heat transfer mechanisms are considered in the vapor region. Thermal conductivity/mass diffusivity are assumed to be a function of temperature/concentration in the heat and concentration equations, respectively. Thermal conductivity and mass diffusivity are assumed to be functions only of temperature and concentration, respectively. Cross-dependence, for example, the dependence of thermal conductivity on concentration, is neglected. Concentration diffusion due to a temperature gradient, i.e., the Soret effect is neglected. Volumetric expansion effects are also neglected.

Based on these assumptions, the mathematical description of the sublimation process in heat and mass transfer phenomena is formulated as follows:

2.2 Mathematical Modeling. Heat transfer during the sublimation process can be modeled by the following conservation equation:

$$\rho c_p\left(\frac{\partial T}{\partial t}+u\frac{\partial T}{\partial x}\right)=\frac{\partial}{\partial x}\left(\kappa(T)\frac{\partial T}{\partial x}\right)+\left(c_{\mathrm{pv}}\frac{dw}{dt}\right)\frac{\partial T}{\partial x},\quad 0<x<s(t) \tag{1}$$

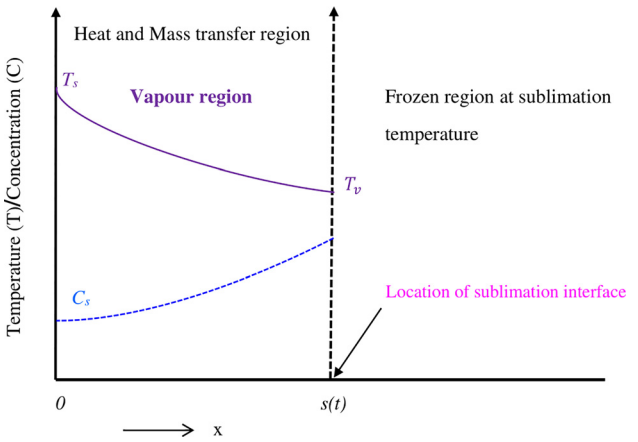

Fig. 1 Schematic diagram of the one-dimensional sublimation process of a wet porous body considered in this work

where $T(x, t)$ is the unknown temperature profile, ρ is density, C_p is specific heat, w stands for water flux, u denotes the unidirectional imposed flow velocity [28,40–45] in the vapor region and C_{pv} is the specific heat of water vapor. $\kappa(T)$ represents the temperature-dependent thermal conductivity [33,46], which is consistent with past work [28]. Two specific temperature dependence functions linear and quadratic are considered in this work as follows

$$\kappa(T) = \kappa_0(1 + b_1(T - T_v)) \text{ and}$$
$$\kappa(T) = \kappa_0(1 + b_1(T - T_v) + b_3(T - T_v)^2) \tag{2}$$

where κ_0 is the bulk thermal conductivity at the sublimation temperature.Similar to the heat transfer equation, mass transport may be modeled by the following conservation equation

$$\frac{\partial C}{\partial t} + u_m \frac{\partial C}{\partial x} = \frac{\partial}{\partial x}\left(D(C)\frac{\partial C}{\partial x}\right), \qquad 0 < x < s(t) \tag{3}$$

where $C(x, t)$ represents the unknown molar concentration distribution of vapor moisture, u_m denotes the unidirectional imposed movement of material due to moisture flow in vapor region. $D(C)$ is the mass diffusivity [47], which similar to the temperature-dependent thermal conductivity in Eq. (2), is assumed to be concentration-dependent as follows:

$$D(C) = D_0(1 + b_2(C - C_s)) \tag{4}$$

where D_0 is the bulk diffusion coefficient at the surface and, b_2 is moisture coefficient of molar concentration. In the sublimation process, it is assumed that the wetted porous body is initially at sublimation temperature T_v and initial molar concentration is C_0, i.e.

$$T(x, t) = T_v, \qquad C(x, t) = C_0, \qquad t = 0 \tag{5}$$

2.2.1 Boundary Condition. At $x = 0$, the temperature and mass for vapor region are subjected to the following conditions:

$$T(x, t) = T_s > T_v, \qquad x = 0 \tag{6}$$

$$C(x, t) = C_s, \quad x = 0 \tag{7}$$

This is indeed the driving function that causes the propagation of the sublimation front.

2.2.2 Heat and Mass Balance Condition. In order to determine the propagation of a moving sublimation front as a function of time, expressions for energy and mass balance at the interface may be written as follows:

$$-k(T)\frac{\partial T}{\partial x} = C_0 M_m L \frac{ds(t)}{dt}, \qquad x = s(t) \tag{8}$$

and

$$D(C)\frac{\partial C}{\partial x} = (C_0 - C(x, t))\frac{ds(t)}{dt}, \qquad x = s(t) \tag{9}$$

where L is the latent heat of sublimation and M_m denotes molar mass of the moisture. In addition, at the sublimation interface, the temperature of the vapor region is equal to the sublimation temperature, i.e.

$$T(x, t) = T_v, \qquad x = s(t) \tag{10}$$

Note that an additional boundary condition for the concentration field at $x = s(t)$, similar to Eq. (10) for the temperature field is not required.

2.3 Dimensionless Scaling Parameters. The mathematical model presented in Sec. 2.2 can be converted into dimensionless form by introducing the following scaling parameters [48]:

$$\theta = \frac{T - T_v}{T_s - T_v}, \quad \grave{C} = \frac{C - C_s}{C_0 - C_s}, \quad \mathrm{Pe}_1 = \frac{u}{\sqrt{\frac{\alpha}{t}}},$$
$$\mathrm{Pe}_m = \frac{u_m}{\sqrt{\frac{D_0}{t}}}, \quad \beta = \frac{c_{pv} C_0 M_m}{\rho c_p} \tag{11}$$

Note that the definitions of Pe_1 and Pe_m assumes that the velocity field decays as $\frac{1}{\sqrt{t}}$. Under the transformations given by Eq. (11), the system of equations with their respective initial and boundary conditions Eqs. (1)–(10), is converted into the following form,

$$\rho c_p\left(\frac{\partial \theta}{\partial t} + u\frac{\partial \theta}{\partial x}\right) = \kappa_0 \frac{\partial}{\partial x}\left((1 + \beta_1\theta)\frac{\partial \theta}{\partial x}\right) + \left(c_{pv}\frac{dw}{dt}\right)\frac{\partial \theta}{\partial x}, \qquad 0 < x < s(t) \tag{12}$$

where $1 + \beta_1\theta$ represents a linear form of thermal conductivity as a function of dimensionless temperature. The rate of moisture flow of the water vapor dw/dt in Eq. (12), can be related to the rate of propagation of the sublimation front as follows [37]:

$$\frac{dw}{dt} \simeq C_0 M_m \frac{ds}{dt} \tag{13}$$

The non-dimensional concentration equation is as follows:

$$\frac{\partial \grave{C}}{\partial t} + u_m \frac{\partial \grave{C}}{\partial x} = D_0 \frac{\partial}{\partial x}\left((1 + \beta_2\grave{C})\frac{\partial \grave{C}}{\partial x}\right), \qquad 0 < x < s(t) \tag{14}$$

Further,

$$-\kappa_0 \frac{\partial \theta}{\partial x} = \frac{C_0 M_m L}{(T_s - T_v)}\frac{ds(t)}{dt}, \qquad x = s(t) \tag{15}$$

$$D_0(1 + \beta_2\grave{C})\frac{\partial \grave{C}}{\partial x} = (1 - \grave{C})\frac{ds(t)}{dt}, \qquad x = s(t) \tag{16}$$

where β_1 and β_2 are dimensionless parameters corresponding to the dimensionless temperature and concentration, respectively. Finally, in the system of Eqs. (12)–(16), the self-similarity space–time transformation is applied as follows:

$$\xi = \frac{x}{2\lambda\sqrt{\alpha t}}, \quad \text{where} \quad s(t) = 2\lambda\sqrt{\alpha t} \tag{17}$$

This results in the following set of ordinary differential equations [49]

$$\frac{d}{d\xi}\left((1 + \beta_1\theta)\frac{d\theta}{d\xi}\right) + 2\lambda(\xi\lambda - Pe_1 + \beta\lambda)\frac{d\theta}{d\xi} = 0, \qquad 0 < \xi < 1 \tag{18}$$

with boundary conditions

$$\theta(0) = 1, \quad \theta(1) = 0 \tag{19}$$

$$\frac{d}{d\xi}\left((1 + \beta_2\grave{C})\frac{d\grave{C}}{d\xi}\right) + \frac{2\lambda}{Lu}\left(\xi\lambda - Pe_m\sqrt{Lu}\right)\frac{d\grave{C}}{d\xi} = 0, \qquad 0 < \xi < 1 \tag{20}$$

with

$$\grave{C}(0) = 0 \tag{21}$$

and

$$\left(1+\beta_2\grave{C}\right)\frac{d\grave{C}}{d\xi}=\frac{2\lambda^2}{Lu}\left(1-C\grave{(}1)\right),\qquad \xi=1 \tag{22}$$

and sublimation interface is given as

$$-\frac{d\theta}{d\xi}=2\lambda^2 l_0,\qquad \xi=1 \tag{23}$$

where $l_0=\frac{C_0 M_m L\alpha}{\kappa_0 (T_s-T_v)}$. Equations (18)–(23) are, in general, nonlinear, and the Legendre wavelet collocation method is used for solving these equations.

3 Numerical Calculations

In this section, we outline the Legendre wavelet collocation method and its working procedure.

3.1 Wavelet. Wavelets constitute a family of functions constructed from dilation and translation of single function called the mother wavelet $\psi(x)$. Wavelets are defined by [50]:

$$\psi_{(\check{a},\check{b})}(\xi)=\frac{1}{\sqrt{|\check{a}|}}\psi\left(\frac{\xi-\check{b}}{\check{a}}\right),\quad \check{a},\check{b}\in\mathbb{R} \tag{24}$$

where $\check{a}$ and $\check{b}$ denote the dilation and translation parameters, respectively.

3.2 Legendre Wavelets. The Legendre polynomials of order m, denoted by $L_m(\xi)$ are defined over the interval $[-1,1]$ on the basis of following recurrence relation [51,52]:

$$\begin{aligned} L_0(\xi)&=1,\\ L_1(\xi)&=\xi,\\ (m+1)L_{m+1}(\xi)&=(2m+1)\xi L_m(\xi)-mL_{m-1}(\xi),\quad m=1,2,3,\ldots \end{aligned} \tag{25}$$

Legendre wavelets $\psi_{nm}(\xi)=\psi(k,\hat{n},m,\xi)$ have four arguments defined on the interval $[0,1)$ by:

$$\psi_{n,m}(\xi)=\begin{cases}\sqrt{m+\frac{1}{2}}\,2^{\frac{k}{2}}L_m\left(2^k\xi-\hat{n}\right), & \frac{\hat{n}-1}{2^k}\le\xi<\frac{\hat{n}+1}{2^k}\\ 0, & \text{otherwise}\end{cases} \tag{26}$$

where $\hat{n}=2n-1$, $n=1,2,\ldots,2^{k-1}$, $k=1,2,3,\ldots$, $m=0,1,2,\ldots,M-1$ is the order of the Legendre polynomials and M is a fixed positive integer and k is any positive integers.

3.3 Function Approximation. Any function $f(\xi)\in L^2[0,1)$ can be expressed in Legendre wavelet series form as follows [53]:

$$f(\xi)=\sum_{n=1}^{\infty}\sum_{m=0}^{\infty}d_{nm}\psi_{n,m}(\xi) \tag{27}$$

where $d_{nm}=\langle f,\psi_{n,m}\rangle$, i.e., inner product between f and ψ. Truncating the infinite series (27) results in

$$f(\xi)=\sum_{n=1}^{2^{k-1}}\sum_{m=0}^{M-1}d_{nm}\psi_{n,m}(\xi)=\mathbf{D}^T\psi(\xi) \tag{28}$$

where

$$\begin{aligned} D=[&d_{10},d_{11},\ldots,d_{1M-1},\ldots,d_{20},d_{21},\ldots,d_{2M-1},\\ &\ldots d_{2^{k-1}0},d_{2^{k-1}1},\ldots,d_{2^{k-1}M-1}]^T \end{aligned} \tag{29}$$

and

$$\begin{aligned} \psi(\xi)=[&\psi_{10},\psi_{11},\ldots,\psi_{1M-1},\ldots,\psi_{20},\psi_{21},\ldots,\\ &\psi_{2M-1},\ldots,\psi_{2^{k-1}0},\psi_{2^{k-1}1},\ldots,\psi_{2^{k-1}M-1}]^T \end{aligned} \tag{30}$$

are matrices of order $2^{k-1}M\times 1$.

3.4 Operational Matrix of Integration. Integration of $\psi(\xi)$, $\xi\in[0,1)$ gives

$$\int_0^{\xi}\psi(s)\,ds=P\,\psi(\xi) \tag{31}$$

where P is the operational matrix of integration of size $2^{k-1}M\times 2^{k-1}M$ which is given in the following manner [50]

$$P=\begin{bmatrix} \frac{1}{2} & \frac{1}{2\sqrt{3}} & 0 & 0 & \ldots & 0 & 0\\ -\frac{1}{2\sqrt{3}} & 0 & \frac{1}{2\sqrt{15}} & 0 & \ldots & 0 & 0\\ 0 & -\frac{1}{2\sqrt{15}} & 0 & \frac{1}{2\sqrt{35}} & \ldots & 0 & 0\\ 0 & 0 & -\frac{1}{2\sqrt{35}} & 0 & \ldots & 0 & 0\\ \ldots & \ldots & \ldots & \ldots & \ldots & \ldots & \ldots\\ \ldots & \ldots & \ldots & \ldots & \ldots & \ldots & \ldots\\ 0 & 0 & 0 & 0 & \ldots & 0 & \frac{1}{2\sqrt{(2M-3)(2M-1)}}\\ 0 & 0 & 0 & 0 & \ldots & -\frac{1}{2\sqrt{(2M-1)(2M-3)}} & 0 \end{bmatrix} \tag{32}$$

3.5 Legendre wavelet Collocation Method. To describe the Legendre wavelet collocation method [52], we consider a nonlinear differential equation of the form

$$\theta''(\xi) = g(\xi, \theta(\xi), \theta'(\xi)) \tag{33}$$

with boundary conditions

$$\theta(0) = A, \quad \theta(1) = B \tag{34}$$

where g is a real valued function for $\xi \in [0, 1)$. Now, we let

$$\theta''(\xi) = \mathbf{D}^T \psi(\xi) \tag{35}$$

Successive integration of Eq. (35) gives

$$\theta'(\xi) = \theta'(0) + \mathbf{D}^T P \psi(\xi) \tag{36}$$

and

$$\theta(\xi) = \theta(0) + \theta'(0)\xi + \mathbf{D}^T P^2 \psi(\xi) \tag{37}$$

Using the boundary conditions (34) into Eq. (37) to obtain

$$\theta'(0) = B - A - \mathbf{D}^T P^2 \psi(1) \tag{38}$$

Substituting Eqs. (35)–(38) into Eq. (33), we arrive at

$$\mathbf{D}^T \psi(\xi) = g(\xi, \theta(\xi), \theta'(\xi)) \tag{39}$$

and the residual $R(\xi, d_1, d_2, d_3, \ldots, d_n)$ can be given as

$$R(\xi, d_1, d_2, d_3, \ldots, d_n) = \mathbf{D}^T \psi(\xi) - g(\xi, \theta(\xi), \theta'(\xi)) \tag{40}$$

Choosing n collocation points $\xi_i, i = 1, 2, 3, \ldots, n$ over (0, 1) so that residual $R(\xi, d_1, d_2, d_3, \ldots, d_n)$ becomes zero. The value of unknown vector $\mathbf{D}$ can be determined with the help of Newton iterative method. Once $\mathbf{D}$ is determined, the solution of the problem is given by Eq. (37).

3.6 Convergence Analysis. In order to understand the accuracy of the numerical method, we investigate the approximate error by introducing orthonormal basis of $L_2[0, 1]$, with M vectors, i.e., $\{\psi_{i,m}\}, m = 0, 1, 2, \ldots, M-1$ defined in Eq. (26) is an orthonormal basis [52,54]. We propose the below theorem to carry out the convergence analysis of the nonlinear problem.

3.6.1 Theorem. Let $\theta_i(\xi)$ be a real valued function defined over (0, 1) for each $i \in \mathbb{N}$ and $\theta_i(\xi)$ is a mth order differential function whose mth derivative is bounded above on (0, 1). Then,
$E_i(\xi) \le \frac{K}{2^m m!}$, where $E_i(\xi) = |\theta_i(\xi) - \check{\theta}_{i,M}(\xi)|$ and $K = sup_{\xi \in [0,1]} \{|\theta_i^m(\xi)|\}$.

Proof: Approximate solution of Eq. (33) is given by Eq. (37) and can be written as

$$\check{\theta}_{i,M}(\xi) = \sum_{m=0}^{M-1} c_{i,M}^T \psi_{i,m}(\xi) \tag{41}$$

$$\begin{aligned} \therefore |\theta_i(\xi) - \check{\theta}_{i,M}(\xi)|^2 &\le |\theta_i(\eta) - \sum_{m=0}^{M-1} c_{i,M}^T \psi_{i,m}(\xi)|^2 \\ &\le |\theta_i(\xi) - \check{\theta}_i^*(\xi)|^2 \end{aligned} \tag{42}$$

where $\check{\theta}_i^*(\xi)$ is an interpolating polynomial of $\check{\theta}_{i,M}(\xi)$. Thus,

$$\begin{aligned} |\theta_i(\xi) - \check{\theta}_{i,M}(\xi)|^2 &\le \int_0^1 \left(\theta_i(\xi) - \check{\theta}_i^*(\xi)\right)^2 d\xi \\ &\le \int_0^1 \left(\frac{1}{2^m m!} sup_{\xi \in [0,1]} \{|\theta_i^m(\xi)|\}\right)^2 d\xi \\ &\quad \text{(using Mean Value Theorem)} \\ &\le \int_0^1 \left(\frac{K}{2^m m!}\right)^2 d\xi = \left(\frac{K}{2^m m!}\right)^2 \end{aligned} \tag{43}$$

i.e.,

$$|\theta_i(\xi) - \check{\theta}_{i,M}(\xi)|^2 \le \left(\frac{K}{2^m m!}\right)^2 \tag{44}$$

Taking the square root on both sides, we get

$$E_i(\xi) \le \frac{K}{2^m m!} \tag{45}$$

From Eq. (45), it is clear that $E_i(\xi)$ approaches zero as m tends to infinity. Equation (45) indicates that in the present computations, increasing the number of Legendre wavelet basis functions is expected to result in reduction of the error. ■

3.7 Working Procedure. The Legendre wavelet collocation as discussed in Sec. 3.4 is used with $M = 5$ and $k = 1$ to solve the problem. Equation (18) may be written as follows [53]:

$$\begin{aligned} &[1 + \beta_1(1 - (1 + \mathbf{D}^T P^2 \psi(1))\xi + \mathbf{D}^T P^2 \psi(\xi))]\mathbf{D}^T \psi(\xi) \\ &\quad + \beta_1(1 + \mathbf{D}^T P^2 \psi(1) - \mathbf{D}^T P \psi(\xi))^2 \\ &\quad - 2\lambda(\lambda\xi - Pe_1 + \beta\lambda)(1 + \mathbf{D}^T P^2 \psi(1) - \mathbf{D}^T P \psi(\xi)) = 0 \end{aligned} \tag{46}$$

Now, we consider residual $R(\xi, d_1, d_2, d_3, \ldots, d_n)$ in the manner

$$\begin{aligned} R(\xi) = &[1 + \beta_1(1 - (1 + \mathbf{D}^T P^2 \psi(1))\xi + \mathbf{D}^T P^2 \psi(\xi))]\mathbf{D}^T \psi(\xi) \\ &+ \beta_1(1 + \mathbf{D}^T P^2 \psi(1) - \mathbf{D}^T P \psi(\xi))^2 \\ &- 2\lambda(\lambda\xi - \mathrm{Pe}_1 + \beta\lambda)(1 + \mathbf{D}^T P^2 \psi(1) - \mathbf{D}^T P \psi(\xi)) \end{aligned} \tag{47}$$

We choose n collocation points $\xi_i, i = 1, 2, 3, \ldots, n$ over (0, 1) so that residual $R(\xi, d_1, d_2, d_3, \ldots, d_n)$ becomes zero. The value of unknown vector $\mathbf{D}$ can be determined with the help of Newton iterative method, and λ can be calculated from energy balance condition Eq. (23). Thus, the tracking of phase change front $s(t)$ can be done using Eq. (17). Similar, procedure is applied to solve the concentration Eq. (20).

4 Verification of Numerical Method

4.1 Linear Case. This section discusses the validation of numerical technique based on Legendre wavelet collocation. Using $\beta_1 = 0$, i.e., a constant thermal conductivity, reduces the present problem to a linear problem. For this special case, an exact solution for Eq. (18) under the boundary condition given by Eq. (19) is available in the past literature [55] as follows:

$$\theta(\xi) = \frac{erf[\mathrm{Pe} - (\xi + \beta)\lambda] - erf[\mathrm{Pe} - (1 + \beta)\lambda]}{erf[\mathrm{Pe} - \beta\lambda] - erf[\mathrm{Pe} - (1 + \beta)\lambda]} \tag{48}$$

For this special case, the corresponding sublimation interface condition Eq. (23) becomes

Table 1 Comparison of position of sublimation interface $s(t)$ obtained by exact and numerical solution for $l_0 = 1, \beta = 1$ and $\mathrm{Pe}_1 = 1, \alpha = 1$, in case of $\beta_1 = 0$ for $M = 5$.

Sr. no.	Parameters	t	$s(t)_{\text{Exact}}$	$s(t)_{\text{Numerical}}$	Relative error
1.	$\beta = 1, \mathrm{Pe}_1 = 1$	0.1	0.428104	0.427720	8.97539×10^{-4}
		0.2	0.605430	0.604887	8.97539×10^{-4}
		0.3	0.741497	0.740832	8.97539×10^{-4}
		0.4	0.856207	0.855439	8.97539×10^{-4}
		0.5	0.957269	0.956410	8.97539×10^{-4}
		0.6	1.048640	1.047690	8.97539×10^{-4}
		0.7	1.132660	1.131640	8.97539×10^{-4}
		0.8	1.210860	1.209770	8.97539×10^{-4}
		0.9	1.284310	1.283160	8.97539×10^{-4}
		1.0	1.353780	1.352570	8.97539×10^{-4}

Table 2 Comparison of position of sublimation interface $s(t)$ obtained by exact and numerical solution for $l_0 = 1, \beta = 1$, $\mathrm{Pe}_1 = 1, \alpha = 1$, in case of $\beta_1 = 0$ for $M = 9$.

Sr. no.	Parameters	t	$s(t)_{\text{Exact}}$	$s(t)_{\text{Numerical}}$	Relative error
1.	$\beta = 1, \mathrm{Pe}_1 = 1$	0.1	0.428104	0.428104	5.84684×10^{-8}
		0.2	0.605430	0.605430	8.26868×10^{-8}
		0.3	0.741497	0.741497	1.01270×10^{-7}
		0.4	0.856207	0.856207	1.16937×10^{-7}
		0.5	0.957269	0.957269	1.30739×10^{-7}
		0.6	1.048640	1.048640	1.43218×10^{-7}
		0.7	1.132660	1.132660	1.54693×10^{-7}
		0.8	1.210860	1.210860	1.65374×10^{-7}
		0.9	1.284310	1.284310	1.75405×10^{-7}
		1.0	1.353780	1.353780	1.84893×10^{-7}

$$\lambda - \frac{e^{-(\mathrm{Pe}-(1+\beta)\lambda)^2}}{\sqrt{\pi}\left(\mathrm{erf}[\mathrm{Pe} - \beta\lambda] - \mathrm{erf}[\mathrm{Pe} - (1+\beta)\lambda]\right)} = 0 \tag{49}$$

For this special case of constant thermal conductivity, results from the full numerical method are compared with the exact solution.

Tables 1 and 2, presents this comparison in terms of sublimation interface location $s(t)$ as a function of time for $l_0 = 1, \beta = 1$, $\mathrm{Pe}_1 = 1, \alpha = 1$. Two cases with $M = 5$ and $M = 9$ are considered. Tables 1 and 2 show excellent agreement between the numerical result and the exact solution for this special case. The relative error between the present work and the exact solution is of the order of 10^{-4} and 10^{-8}, respectively. This improvement in error with increasing order of the matrix is consistent with Theorem 3.6.1. In addition to Tables 1 and 2, comparison between the numerical method and exact solution for the special case is also presented in Fig. 2, in which, the temperature distribution θ is plotted and compared for $l_0 = 1, \beta = 1, \mathrm{Pe}_1 = 1, \alpha = 1$ at $M = 9$. Figure 2 shows excellent agreement with an exact solution for temperature distribution. The two curves are nearly identical, with an extremely small error of the order of 10^{-8} between the two.

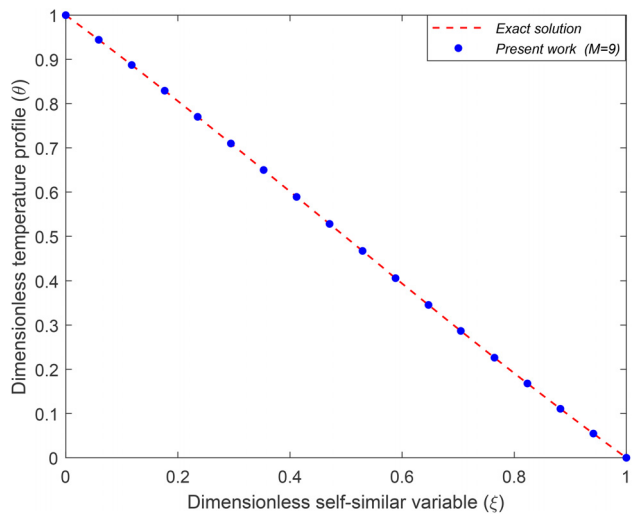

Fig. 2 Comparison of dimensionless temperature θ profile between the numerical method and exact solution for the special case of $l_0 = 1, \beta = 1, \mathrm{Pe}_1 = 1, \alpha = 1$ at $M = 9$

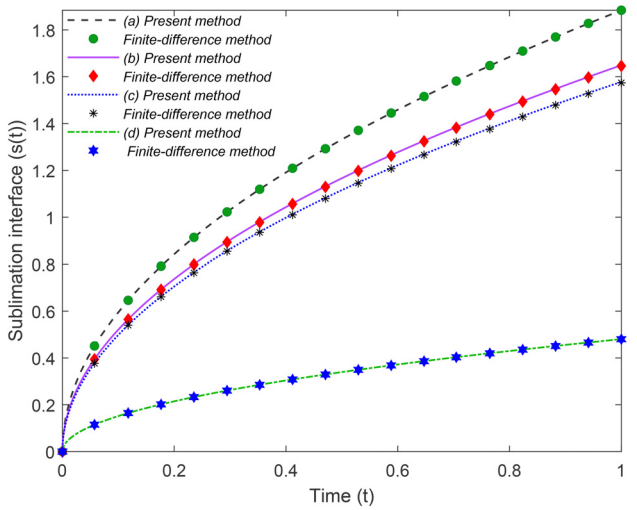

Fig. 3 Comparison of sublimation interface $(s(t))$ between the present numerical method with $M = 5$ and finite-difference method

4.2 Non-Linear Case. To validate the current numerical method for a full nonlinear model, we compare our results with the well-documented finite difference method [56–58]. To verify our numerical method, we consider Eqs. (17)–(19) and (23). A central-difference scheme is used for first- and second-order derivatives with respect to space. We compare our numerical method for $M = 5$, while a step size $h = 0.05$ is taken for finite difference method. A comparison between the two is shown in Fig. 3. The parameter values (from the top of the curve to the bottom) are taken as: (a) $l_0 = 0.5, \beta_1 = 0.2$, $\mathrm{Pe}_1 = 0.5, \beta = 0.1$; (b) $l_0 = 0.5, \beta_1 = 0.2, \mathrm{Pe}_1 = 0.8, \beta = 1.0$; (c) $l_0 = 1.0, \beta_1 = 0.7$, $\mathrm{Pe}_1 = 0.5, \beta = 0.1$; (d) $l_0 = 10, \beta_1 = 0.2$, $\mathrm{Pe}_1 = 0.5, \beta = 0.5$. From Fig. 3, it is found that results obtained from the current numerical technique are in excellent agreement with the finite difference method.

5 Results and Discussion

Computations for the nonlinear sublimation problem based on the Legendre wavelet collocation method are carried out using Mathematica computing software. The numerical procedure utilized for this work is shown in Fig. 4. The impact of a number of nondimensional parameters on the nature of the sublimation process is discussed in Secs. 5.1–5.7. The range of β_1 is taken from 0 to 1, Pe_1 from 0.1 to 0.8, β from 0.1 to 2.5, l_0 from 1 to 100, β_2 from 0 to 1, Pe_m from 0.05 to 1.5 and Lu from 0.05 to 3.5.

5.1 Impact of Temperature-Dependent Thermal Conductivity on Sublimation Process. The thermal conductivity of a material is, in general, a function of the local temperature. With increasing temperature, molecular and structural vibrations increase, which generally result in greater phonon propagation and, thus, greater thermal conductivity. In this work, a linear temperature dependence is assumed, and, therefore, the temperature-dependent thermal conductivity, represented by the

nondimensional parameter β_1 is of key interest. In order to characterize the impact of temperature-dependent thermal conductivity on the sublimation process, the dimensionless temperature profile within the sublimation region and the location of the sublimation interface as a function of time are computed. Fig. 5(*a*) presents the effect of $\beta_1(0.0, 0.1, 0.3, 0.5, 0.7, 1.0)$ on the temperature distribution θ as a function of the self-similarity variable ξ with $\mathrm{Pe}_1 = 0.5, \beta = 0.1$ and $l_0 = 1$. Since ξ contains both x and t, therefore, the plot represents both spatial and temporal variation of the temperature distribution. These plots show that with an increasing value of β_1, the temperature within the sublimated region increases gradually. An explanation for this observation is that increasing β_1, results in faster molecular propagation of heat and, thus, a greater rate of sublimation. Note that, $\beta_1 = 0$ reduces the model to a constant thermal conductivity scenario, for which, analysis is already available in the literature [28]. The impact of dimensionless temperature parameter β_1 on the growth of the sublimation interface is shown in Fig. 5(*b*). All parameter values are the same as Fig. 5(*a*). It is seen that the sublimation front propagates faster and faster with an increasing value of β_1 as expected.

In addition to the effect of linear form of the temperature-dependent thermal conductivity on sublimation process, a quadratic form of the temperature-dependent thermal conductivity is also carried out and written in the form of $1 + \beta_1\theta + \gamma_1\theta^2$. Figure 6(*a*) depicts the effect of $\gamma_1(0.3, 0.5, 0.7, 1.0)$ on the temperature configuration θ at $\mathrm{Pe}_1 = 0.5, \beta = 0.1$, $l_0 = 1$, and $\beta_1 = 0.1$. This plot shows that increasing the value of γ_1, the temperature within the sublimation region goes up. It is also seen that the rate of increase in the temperature field is of a quadratic nature. Further, increasing the value of γ_1 results in faster propagation rate of the sublimation interface as shown in Fig. 6(*b*). Consequently, rate of sublimation increases with increasing γ_1.

Based on this, it may be concluded that sublimation occurs faster when thermal conductivity is strongly temperature-dependent and increases with temperature, compared to a baseline constant thermal conductivity case. Accounting for temperature-dependent thermal conductivity is important for the modeling of various industrial processes, such as thermal/cold energy storage systems, the preservation of biological tissue, and food

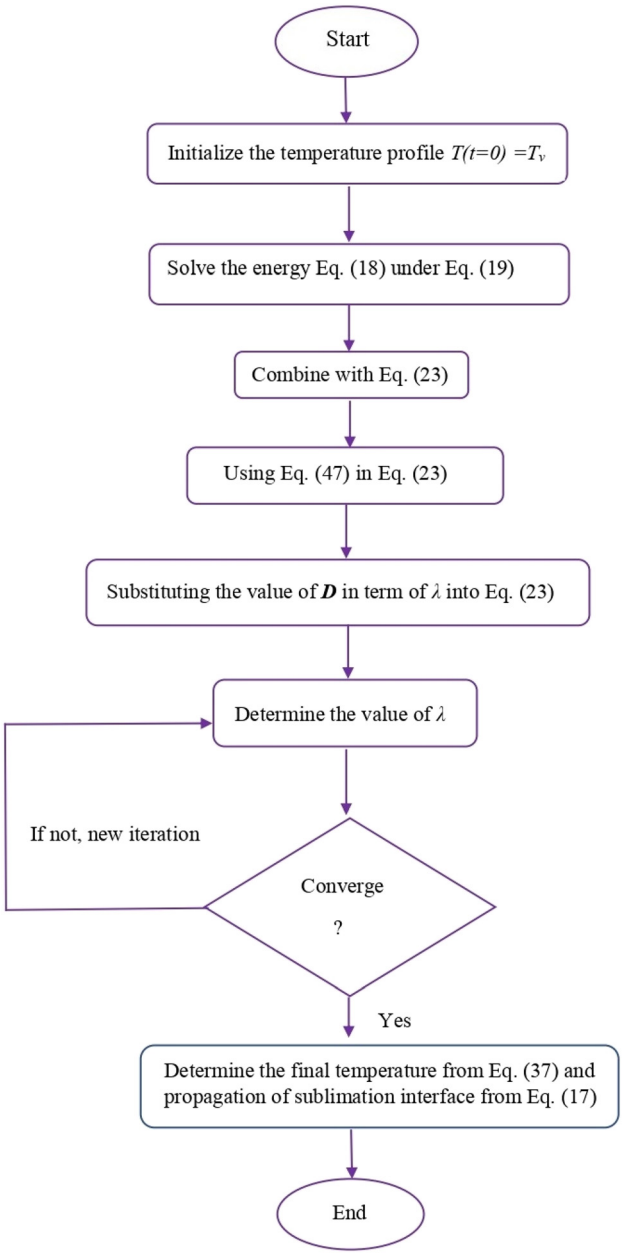

Fig. 4 Outline of the numerical procedure using the Legendre wavelet collocation method

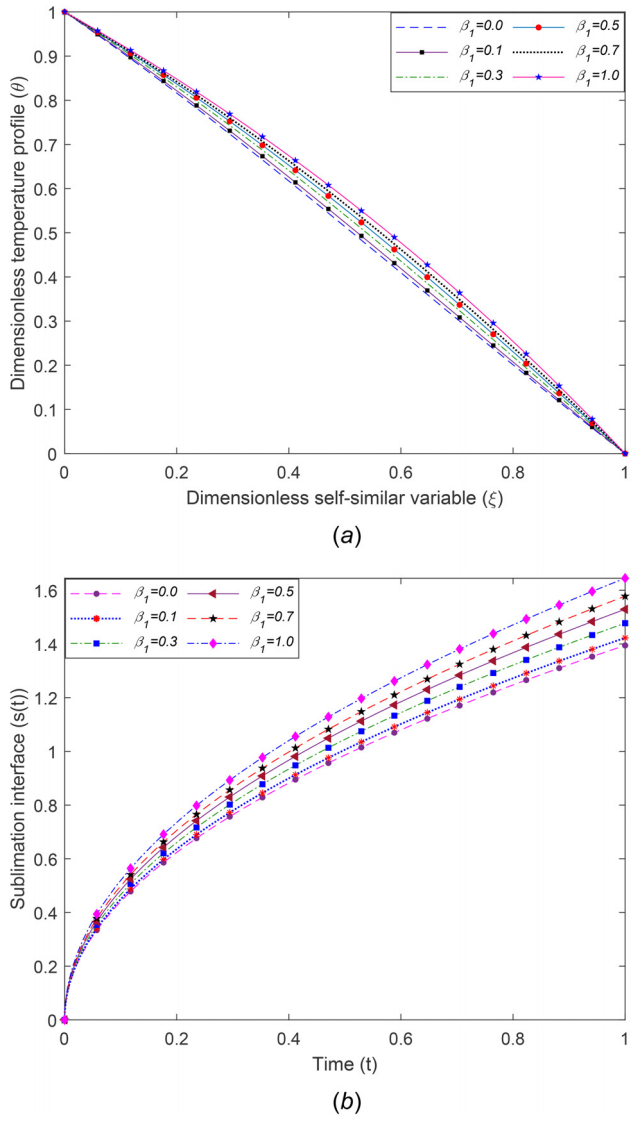

Fig. 5 Effect of dimensionless parameter β_1 on dimensionless temperature profile and sublimation interface at $\mathrm{Pe}_1 = 0.5$, $\beta = 0.1$, $l_0 = 1, \alpha = 1$

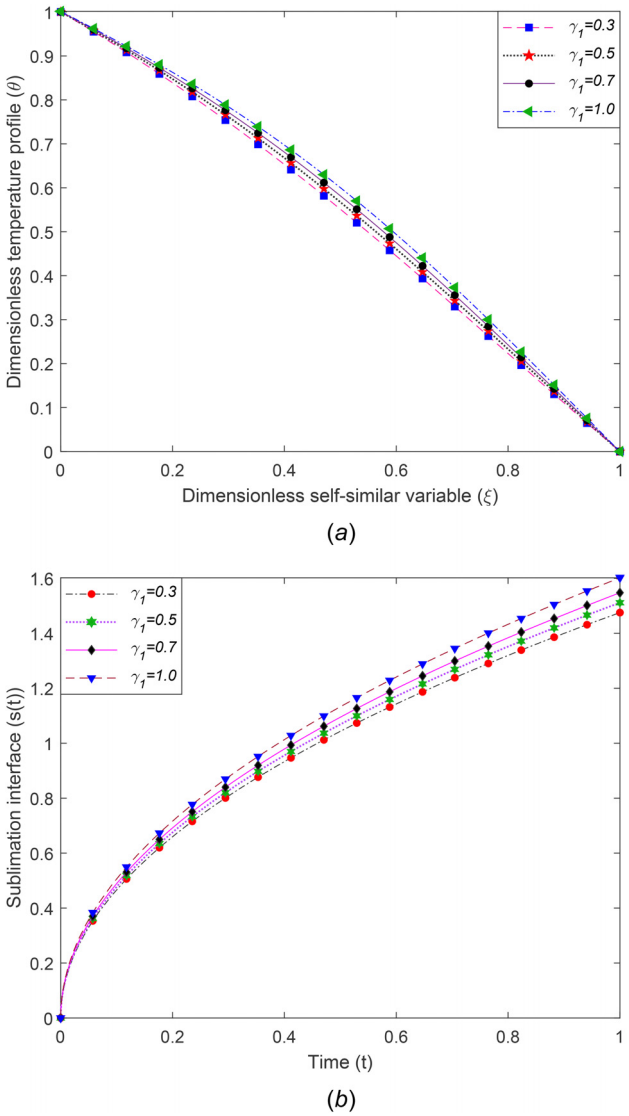

Fig. 6 Effect of dimensionless parameter γ_1 on dimensionless temperature profile and sublimation interface at $Pe_1 = 0.5$, $\beta = 0.1$, $l_0 = 1$, $\alpha = 1$, $\beta_1 = 0.1$

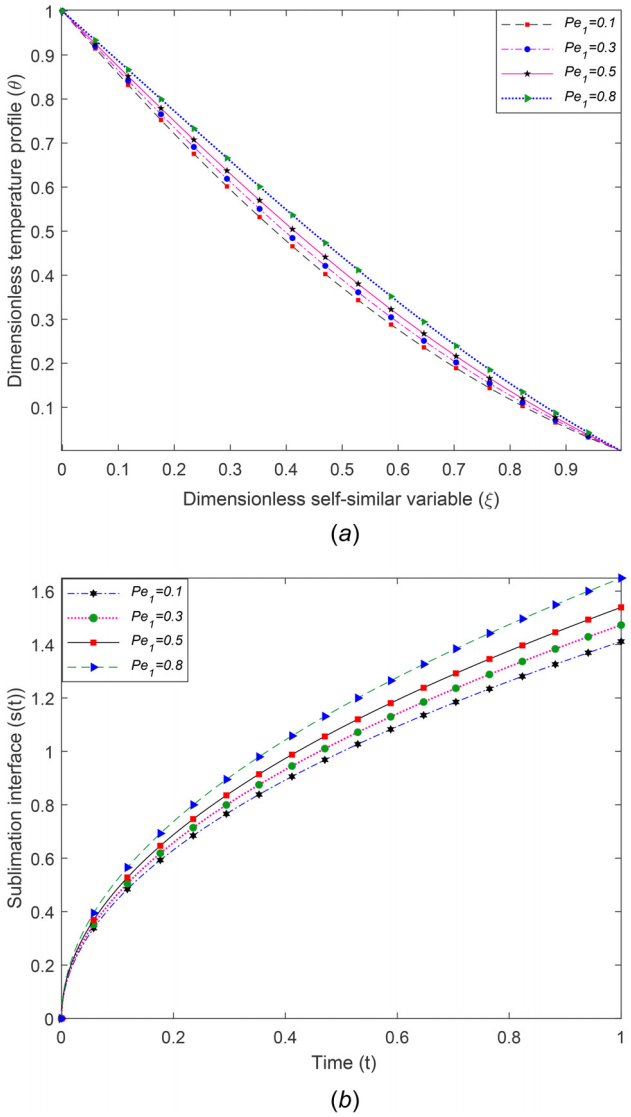

Fig. 7 Effect of Péclet number Pe_1 on dimensionless temperature profile and sublimation interface at β_1=0.2, β=1, l_0=0.5, α=1

technology. While the present analysis is limited to a linearly increasing thermal conductivity, such linearization is reasonable for several applications, especially when the temperature change is relatively small. Conclusions similar to those drawn here may also be expected for other forms of temperature-dependent thermal conductivity.

5.2 Impact of Convection in Terms of Péclet Number Pe_1. The impact of convection on the sublimation process is investigated next. Convection is represented in this work by the nondimensional Péclet number (Pe_1). Convection is a key feature of several heat and mass transfer problems. It arises due to the imposed advective movement of molecules, as opposed to diffusive transport that leads to conduction heat transfer. Forced convection is often dominant over diffusive conduction and, therefore, is important to study. The Péclet number is a dimensionless ratio of the advective transport of a material to the rate of diffusive transport. Figure 7(*a*) presents the effect of varying the Péclet number Pe_1 on the dimensionless temperature profile θ at $\beta_1 = 0.2, l_0 = 0.5, \beta = 1$ within the sublimation region ξ. These plots show that as the value of the Péclet number increases, temperature within the sublimation region also goes up, as expected. The impact of convection on the propagation of the sublimation interface is illustrated in Fig. 7(*b*). This figure shows more and more rapid propagation of the sublimation interface for a larger value of the Péclet number. This is fundamentally due to the greater rate of convection of thermal energy to the sublimation front when the Péclet number increases, resulting in faster sublimation. This result is similar to the observations reported by Jitendra et al. [28].

In view of the strong impact of the Péclet number observed in Figs. 7(*a*) and 7(*b*), convective heat transfer is identified as a key process that influences the sublimation process and should be enhanced when a greater rate of sublimation is desired in applications such as AFD.

5.3 Impact of Convection Due to Mass Transfer of Water Vapor on Sublimation Process in Terms of Dimensionless Parameter β. The rate of sublimation of wet materials also depends on the transfer of water vapor evaporating through the dried region to the gas phase. Therefore, consideration of water vapor transfer is necessary in studying the sublimation problem. In this work, convection arising due to mass transfer of water vapor during sublimation is represented by the dimensionless parameter β. The impact of β on the sublimation process is

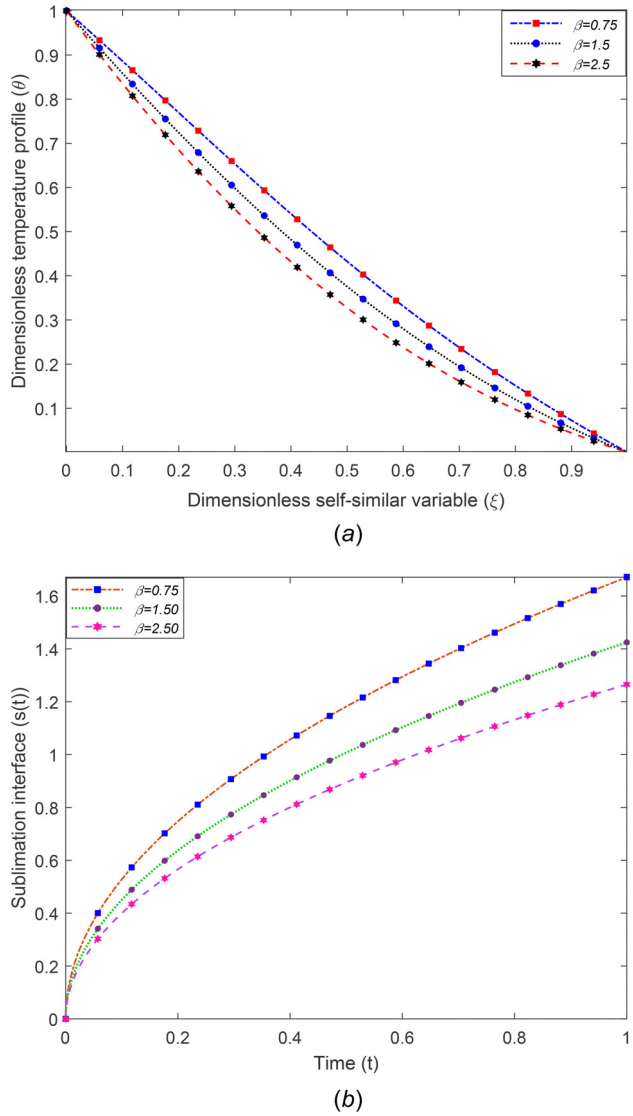

Fig. 8 Effect of convective term β on dimensionless temperature profile and sublimation interface at $\beta_1 = 0.2, \mathrm{Pe}_1 = 0.5, l_0 = 0.5, \alpha = 1$

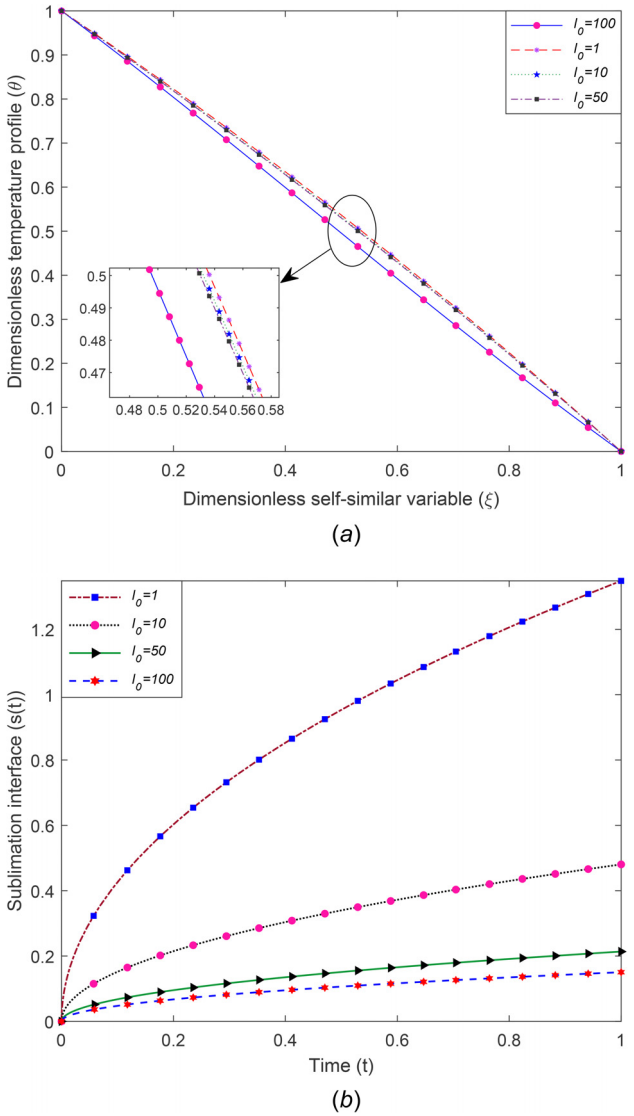

Fig. 9 Effect of dimensionless latent heat of sublimation l_0 on dimensionless temperature profile and sublimation interface at $\beta = 0.5, \mathrm{Pe}_1 = 0.5, \beta_1 = 0.2, \alpha = 1$

discussed in Figs. 8(*a*) and 8(*b*). Specifically, the effect of variation of β on the dimensionless temperature profile θ is presented in Fig. 8(*a*) and the impact of the propagation of the sublimation front is presented in Fig. 8(*b*). Other problem parameters are $\beta_1 = 0.2, l_0 = 0.5$ and $\mathrm{Pe}_1 = 0.5$. These plots show a reduction in the temperature field and rate of propagation of the sublimation front with increasing value of β. This situation occurs because when β increases, more energy is needed to evaporate the water from the wet material. This results in greater energy needed for temperature rise and, therefore, a lower temperature response. Due to the lower temperature field, the propagation rate of the sublimation interface is also correspondingly lower. Consequently, convection produced by mass transfer due to water vapor has only a weak impact on sublimation rate.

5.4 Effect of Dimensionless Latent Heat of Sublimation l_0 on Sublimation Process. The latent heat of sublimation is the amount of heat required to convert a unit mass of solid into gas. Clearly, the dimensionless heat of sublimation l_0 plays a key role in determining the rate of the sublimation process, similar to the latent heat of melting and solidification in traditional melting/solidification heat transfer problems. Figure 9(*a*), presents the effect of varying l_0 on the temperature profile θ with $\beta = 0.5, \mathrm{Pe}_1 = 0.5, \beta_1 = 0.2$. In order to illustrate this further, Fig. 9(*b*) plots the impact of l_0 on the sublimation front propagation with time. It is found that increasing the value of l_0 results in a small reduction in the temperature profile. Further, there is a reduction in sublimation front propagation with increasing value of l_0. This is consistent with the physical nature of the problem, wherein a large value of l_0 implies greater heat needed for sublimation of a unit mass and, therefore, a slower rate of propagation of the sublimation front. A saturation effect is observed here, in that there is a strong reduction in propagation when going from $l_0 = 1$ to $l_0 = 10$, but much reduced impact at greater values, for example, when going from $l_0 = 50$ to $l_0 = 100$.

5.5 Impact of Concentration-Dependent Mass Diffusivity on Sublimation Process in Terms of Dimensionless Moisture Concentration Parameter β_2. The moisture diffusion coefficient models the mass flowrate of water with respect to time and space. The concentration-dependent mass diffusivity is an important property that should be accounted for in modeling the sublimation of a wet porous material. This is essential for assessing the rate of water dispersion in the sublimation region during the initial

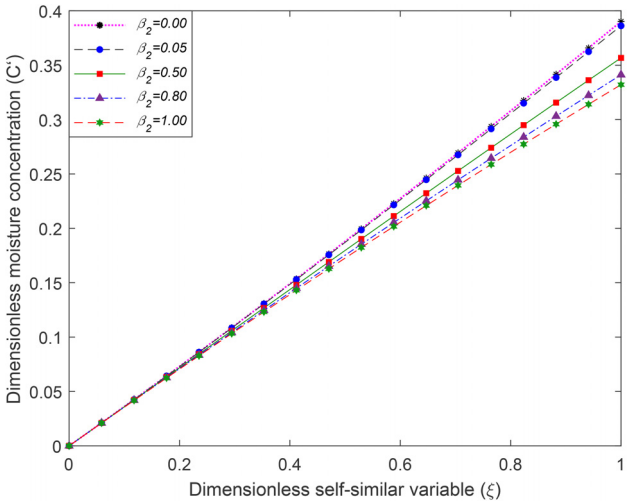

Fig. 10 Effect of β_2 on dimensionless moisture concentration C at Lu = 0.5, Pe_m = 0.4, λ = 0.2

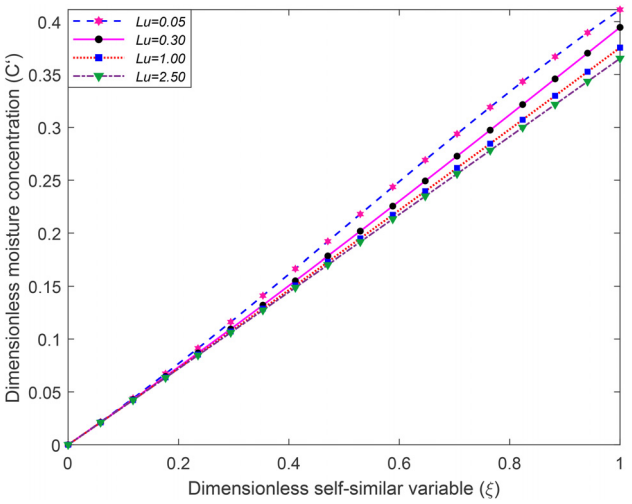

Fig. 12 Effect of Lu on dimensionless moisture concentration C at Pe_m = 0.5, β_2 = 0.2, λ = 0.2

process from high to low concentrations. Figure 10 illustrates the effect of variation of moisture concentration parameter β_2 on dimensionless concentration profile $\grave{C}$ at Lu = 0.5, Pe_m = 0.4, λ = 0.2. As the value of β_2 increases, Fig. 10 shows that the moisture concentration within the sublimation region decreases gradually. Clearly, at a certain moisture concentration, the sublimation process speeds up with increase in β_2. Moreover, as the value of β_2 decreases, results from the present work gets closer and closer to the constant mass diffusivity case $\beta_2 = 0$, as expected. From this figure, it can also be observed that concentration-dependent mass diffusivity has a more pronounced impact on the sublimation process than constant moisture diffusivity.

This is an important result for industrial processes such as AFD because the moisture diffusivity of most materials of interest is expected to be concentration-dependent.

5.6 Impact of Moisture Concentration Driven Convection on Sublimation Process in Terms of Péclet Number Pe_m. Convective mass transfer involves mass flow between an interface and a moving fluid or between two relatively immiscible moving fluids. Therefore, convective mass transfer is expected to be an important parameter that impacts the sublimation process.

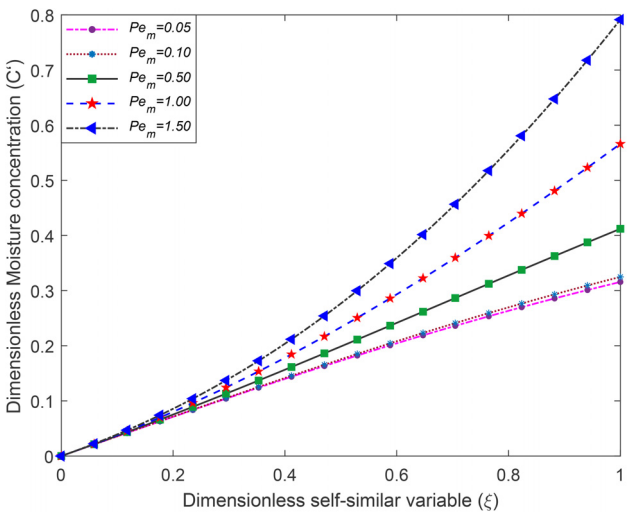

Fig. 11 Effect of Pe_m on dimensionless moisture concentration C at Lu = 0.1, β_2 = 0.2, λ = 0.2

Figure 11 presents the impact of convective moisture flow in terms of Péclet number Pe_m on dimensionless concentration profile $\grave{C}$ at Lu = 0.1, β_2 = 0.2, λ = 0.2. It is observed that as the value of Pe_m increases, the moisture concentration rate increases. This observation is explained on the basis of the slower movement of molecules, since molecules lose greater energy in converting the amount of molar mass into gaseous form. Consequently, the sublimation process is slowed down by increasing the rate of convective mass transfer.

5.7 Analysis of Ratio of Moisture Diffusivity to the Thermal Diffusivity on Sublimation Process in Term of Luikov Number Lu. Thermal diffusion and mass diffusion both occur in parallel in heat and mass transfer problems involving the sublimation of a porous body. In this situation, the ratio of mass diffusivity to heat diffusivity is represented by the Luikov number, which is expected to affect the transition rate of the sublimation process. In this work, the effects of Luikov number Lu on dimensionless concentration profile $\grave{C}$ at Pe_m = 0.5, β_2 = 0.2, λ = 0.2 is presented in Fig. 12. The greater value of Lu, greater is the rate of moisture diffusion away from the phase interface, and thus

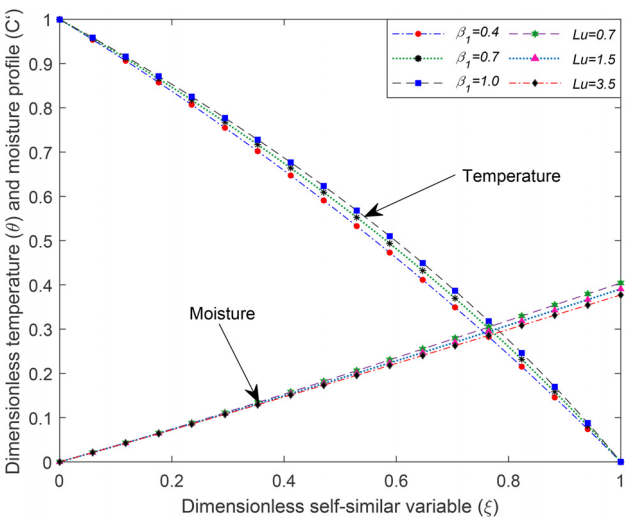

Fig. 13 Effect of β_1 on dimensionless temperature profile and effect of Lu on dimensionless moisture concentration C at Pe_1 = 0.5, β = 0.1, λ = 0.4, l_0 = 1.0 and Pe_m = 0.5, β_1 = 0.2, λ = 0.4, respectively

the flatter is the molar concentration gradient needed for the mass diffusion. Figure 13 shows that, by increasing the value of the Luikov number, the rate of the dimensionless concentration profile decreases.

Finally, Fig. 13 presents the simultaneous impact of β_1 on the temperature distribution and the impact of Lu on the moisture concentration distribution. Parameter values are $\mathrm{Pe}_1 = 0.5, \beta = 0.1$, $l_0 = 1.0$, $\mathrm{Pe}_m = 0.5, \beta_1 = 0.2$. From this figure, it is evident that for the fixed value of $\lambda = 0.4$, as β_1 increases, temperature increases, while the opposite trend is obtained for the Luikov number. By increasing the value of β_1, kinetic energy of the molecules accelerates the transition process, resulting in a high temperature response within the region, while by increasing the value of Lu, mass diffusivity increases and hence concentration decreases.

6 Conclusions

Understanding the nature of the sublimation process is critical for improving and optimizing heat/mass transfer during various engineering processes, such as thermal management and food processing. Heat and mass transfer problems involving single or double moving interfaces are particularly complicated and interesting in the case of temperature- and mass-dependent thermophysical properties. The present study contributes towards understanding and improving such practical problems by considering the case of linearly/quadratically changing properties. Such linearization is a reasonable model for several practical processes, especially when the temperature change is relatively small. In general, mass diffusivity is usually a function of concentration and not temperature, just as thermal conductivity is usually a function of temperature and not concentration. Moreover, ignoring the temperature dependence of mass diffusivity is a necessary assumption for two reasons. Doing so uncouples the mass transfer and heat transfer problems and prevents the problem from becoming highly nonlinear. As the focus of the present work is to derive an analytical solution, this effect has been ignored. Further, the numerical technique developed here is equally applicable to other types of temperature dependence as well. In addition to good agreement with exact solution for a special case, the convergence analysis of this nonlinear problem is also presented. The present numerical code is validated with an exact solution and finite difference computations in the case of a full nonlinear model. Key conclusions of the present work are as follows:

- The rate of sublimation is enhanced by increasing the dimensionless temperature parameter β_1 and γ_1. This may have direct relevance to the preservation of biological materials and other related heat/mass transfer processes.
- Concentration-dependent moisture diffusivity has a more pronounced impact on sublimation process than a fixed moisture diffusivity. Therefore, similar to temperature-dependent thermal conductivity, it is an important parameter to consider in practical industrial processes.
- An increased value of Pe_1 is found to enhance the rate of sublimation, as expected, while, increasing the latent heat of sublimation l_0 is found to result in slower sublimation. Similar observations are made for the convective mass transfer Pe_m and Luikov number Lu.

Observations from the present study improve the theoretical and mathematical understanding of an important and industrially relevant heat and mass transfer problem. Potential applications may be found in a variety of problems, such as microwave freeze drying, energy storage systems, and thermal management. In addition, the techniques developed in this work may be applicable for the analysis of other related nonlinear problems in heat and mass transfer involving moving interfaces.

Acknowledgment

Vikas Chaurasiya is grateful to DST (INSPIRE)-New Delhi (India) for the Senior Research Fellowship vide Ref. No. DST/INSPIRE/03/2017/000184 (i) Ref. no/Math/2017-18/March 18/347.

Data Availability Statement

No data, models, or code were generated or used for this paper.

Nomenclature

Thermophysical Properties

C = molar concentration of vapor moisture (mol m^{-3})
c_p = specific heat (Jkg^{-1}K^{-1})
c_{pv} = specific heat of water vapor (Jkg^{-1}K^{-1})
D_0 = bulk mass diffusivity (m^{2}s^{-1})
K = thermal conductivity (Wm^{-1}K^{-1})
L = latent heat of sublimation (J kg^{-1})
M_m = molar mass (kg mol^{-1})
p_v = vapor pressure (Pa)
R_0 = universal gas constant (J mol^{-1} K^{-1})
t = time (s)
u = uni-directional velocity (m s^{-1})
α = thermal diffusivity (m^{2}s^{-1})
ρ = material density (kg m^{-3})

Temperature Profile

b_1 = temperature parameter (K^{-1})
b_2 = concentration parameter (mol^{-1} m^3)
b_3 = temperature parameter (K^{-2})
$\grave{C}$ = non-dimensional molar concentration ($\grave{C} = \frac{C-C_s}{C_0-C_s}$)
T = temperature (K)
T_v = sublimation temperature (K)
T_s = surface temperature (K)
θ = non-dimensional temperature profile ($\theta = \frac{T-T_v}{T_s-T_v}$)

Space Variables

x = space coordinate (m)
$s(t)$ = moving sublimation front (m)
ξ = non-dimensional self-similar variable

Non-Dimensional Quantities

β = non-dimensional quantity ($\beta = \frac{c_{\mathrm{pv}} M_m C_0}{c_p \rho}$)
l_0 = non-dimensional latent heat of sublimation ($l_0 = \frac{C_0 M_m L \alpha}{\kappa_0 (T_s - T_v)}$)
λ = unknown constant ($\lambda = \frac{s(t)}{2\sqrt{\alpha t}}$)
β_1 = dimensionless temperature parameter ($\beta_1 = b_1(T_s - T_v)$)
β_2 = dimensionless concentration parameter ($\beta_2 = b_2(C_0 - C_s)$)
γ_1 = dimensionless temperature parameter ($\gamma_1 = b_3(T_s - T_v)^2$)

Non-Dimensional Numbers

Pe_1 = Péclet number ($\mathrm{Pe}_1 = \frac{u}{\sqrt{\frac{\alpha}{t}}}$)
Pe_m = Péclet number ($\mathrm{Pe}_m = \frac{u}{\sqrt{\frac{D_0}{t}}}$)
Lu = Luikov number ($\mathrm{Lu} = \frac{D_0}{\alpha}$)

Subscripts

0 = initial
m = moisture
s = surface $x = 0$

References

[1] Reddy, Y. D., Mebarek-Oudina, F., Goud, B. S., and Ismail, A. I., 2022, "Radiation, Velocity and Thermal Slips Effect Toward Mhd Boundary Layer Flow Through Heat and Mass Transport of Williamson Nanofluid With Porous Medium," Arabian J. Sci. Eng., **47**, pp. 16355–16369.
[2] Hindmarsh, R. C. A., Van Der Wateren, F. M., and Verbers, A. L. L. M., 1998, "Sublimation of Ice Through Sediment in Beacon Valley, Antarctica," Geografiska Annaler: Ser. A, Phys. Geography, **80**, pp. 209–219.
[3] Tung, H. S., Guan, Z. Y., Liu, T. Y., and Chen, H. Y., 2018, "Vapor Sublimation and Deposition to Build Porous Particles and Composites," Nat. Commun., **9**, p. 2564.

[4] Mandal, S., and Kulkarni, B. D., 2011, "Separation Strategies for Processing of Dilute Liquid Streams," Int. J. Chem. Eng., **2011**, p. 659012.
[5] Wang, W., Yang, J., Hua, D., Hua, Y., Wanga, S., and G, C., 2018, "Experimental and Numerical Investigations on Freeze-Drying of Porous Media With Prebuilt Porosity," Chem. Phys. Lett., **700**, pp. 80–87.
[6] Srikiatden, J., Robertsand, J. S., D, H., Hua, Y., Wanga, S., and Chen, S., 2007, "Moisture Transfer in Solid Food Materials:A Review of Mechanisms, Models, and Measurements," Int. J. Food Prop., **10**(4), pp. 739–777.
[7] Upadhyay, S., and Rai, K. N., 2018, "A New Iterative Least Square Chebyshev Wavelet Galerkin Fem Applied to Dual Phase Lag Model on Microwave Drying of Foods," Int. J. Therm. Sci., **139**, pp. 217–231.
[8] Jumikis, A. R., 1967, "Upward Migration of Soil Moisture by Various Mechanisms Upon Freezing," Phys. Snow Ice: Proc., **1**(2), pp. 1387–1399.
[9] Rani, P., and Tripathy, P. P., 2020, "Modelling of Moisture Migration During Convective Drying of Pineapple Slice Considering Non-Isotropic Shrinkage and Variable Transport Properties," J. Food Sci. Technol., **57**, p. 3748.
[10] Labuza, T. P., and Hyman, C. R., 1998, "Modelling of Moisture Migration During Convective Drying of Pineapple Slice Considering Non-Isotropic Shrinkage and Variable Transport Properties," Trends Food Sci. Technol., **9**(2), pp. 47–55.
[11] Singh, A. K., Singh, R., and Chaudhary, D. R., 1999, "Heat Conduction and Moisture Migration in Unsaturated Soils Under Temperature Gradients," Pramana, **33**, p. 587.
[12] Ansar, Sukmawaty, Murad, Ulfa, M., and Azis, A. D., 2022, "Using of Exhaust Gas Heat From a Condenser to Increase the Vacuum Freeze-Drying Rate," Results Eng., **13**, p. 100317.
[13] Alexiades, V., 1993, *Mathematical Modeling of Melting and Freezing Processes*, Taylor and Francis Group, New York.
[14] Speight, J. G., 2018, *Reaction Mechanisms in Environmental Engineering: Analysis and Prediction*, Elsevier, Oxford, UK.
[15] Jambon-Puillet, E., Shahidzadeh, N., and Bonn, D., 2018, "Singular Sublimation of Ice and Snow Crystals," Nat. Commun., **9**, p. 4191.
[16] Peng, S. W., Qin, Q. H., and Cheng, S. M., 1992, "Exact Solution of Coupled Heat and Mass Transfer With Double Moving Interfaces in a Porous Half-Space, Part 1: Mass Transfer Controlled by the Fick's Law," Int. J. Energy Res., **9**(5), pp. 387–400.
[17] Fedorov, V. A., Zhukov, E. G., Nikolashin, S. V., Potolokov, V. N., Serov, A. V., and Smetanin, A. V., 2001, "Sublimation Purification of Crude Arsenic Recovered From Nonferrous Waste," Int. J. Energy Res., **37**, pp. 1011–1016.
[18] Chaurasiya, V., Chaudhary, R. K., Wakif, A., and Singh, J., 2022, "A One-Phase Stefan Problem With Size-Dependent Thermal Conductivity and Moving Phase Change Material Under the Most Generalized Boundary Condition," Waves Random Complex Media.
[19] Chaurasiya, V., Chaudhary, R. K., Awad, M. M., and Singh, J., 2022, "A Numerical Study of a Moving Boundary Problem With Variable Thermal Conductivity and Temperature-Dependent Moving Pcm Under Periodic Boundary Condition," Eur. Phys. J. Plus, **137**, p. 714.
[20] Luikov, A. V., 1975, "Systems of Differential Equations of Heat and Mass Transfer in Capillary-Porous Bodies," Int. J. Heat Mass Transfer, **18**(1), pp. 1–14.
[21] Cho, S. H., 1975, "An Exact Solution of the Coupled Phase Change Problem in a Porous Medium," Int. J. Heat Mass Transfer, **18**(10), pp. 1139–1142.
[22] Mikhailov, M. D., 1975, "Exact Solution of Temperature and Moisture Distributions in a Porous Half-Space With Moving Evaporation Front," Int. J. Heat Mass Transfer, **18**(6), pp. 797–804.
[23] Mikhailov, M. D., 1976, "Exact Solution for Freezing of Humid Porous Half-Space," Int. J. Heat Mass Transfer, **19**(6), pp. 651–655.
[24] Lin, S., 1981, "An Exact Solution of the Sublimation Problem in a Porous Medium," ASME J. Heat Mass Transfer-Trans. ASME, **103**(1), pp. 165–168.
[25] Lin, S., 2002, "Exact Solution for Determination of the Maximum Sublimation Rate in a Porous Medium," ASME J. Heat Mass Transfer-Trans. ASME, **124**(3), pp. 525–529.
[26] Peng, S. W., Qin, Q. H., Cheng, S. M., and Chen, G. Q., 1992, "Exact Solution of Coupled Heat and Mass Transfer in a Porous-Half Space. part 2: Mass Transfer Controlled by Fick and Darcy Law," Int. J. Energy Res., **16**(5), pp. 401–411.
[27] Peng, S. W., and Chen, G. Q., 1993, "Exact Solution of Coupled Heat and Mass Transfer With Double Moving Interfaces in a Porous-Half Space, Part 3: Effect of Surface Pressure and Permeability on Rates of Sublimation and Desorption," Int. J. Energy Res., **17**(3), pp. 193–202.
[28] Jitendra, Rai, K. N., and Singh, J., 2022, "An Analytical Study on Sublimation Process in the Presence of Convection Effect With Heat and Mass Transfer in Porous Medium," Int. Commun. Heat Mass Transfer, **131**, p. 105833.
[29] Zhang, C., Bu, X., He, J., Liu, C., Lin, G., and Miao, J., 2020, "Simulation of Evaporation and Sublimation Process in Porous Plate Water Sublimator Based on a Reduced Cfd Model," Int. J. Heat Mass Transfer, **154**, p. 119787.
[30] Wang, Z. H., and Shi, M. H., 1998, "The Effects of Sublimation-Condensation Region on Heat and Mass Transfer During Microwave Freeze Drying," ASME J. Heat Mass Transfer-Trans. ASME, **120**(3), pp. 654–660.
[31] Jafari, H., Hosseinzadeh, H., Gholami, M. R., and Ganj, D. D., 2017, "Application of Homotopy Perturbation Method for Heat and Mass Transfer in the Two-Dimensional Unsteady Flow Between Parallel Plates," Int. J. Appl. Comput. Math., **3**, pp. 1677–1688.
[32] Parhizi, M., and Jain, A., 2019, "Solution of the Phase Change Stefan Problem With Time-Dependent Heat Flux Using Perturbation Method," ASME J. Heat Mass Transfer-Trans. ASME, **141**(2), p. 024503.
[33] Singh, J., Jitendra., and Rai, K. N., 2020, "Legendre Wavelet Based Numerical Solution of Variable Latent Heat Moving Boundary Problem," Math. Comput. Simul., **178**, pp. 485–500.
[34] Chaurasiya, V., Kumar, D., Rai, K. N., and Singh, J., 2020, "A Computational Solution of a Phase-Change Material in the Presence of Convection Under the Most Generalized Boundary Condition," Therm. Sci. Eng. Prog., **20**, p. 100664.
[35] Djebali, R., Mebarek-Oudina, F., and Rajashekhar, C., 2021, "Similarity Solution Analysis of Dynamic and Thermal Boundary Layers: Further Formulation Along a Vertical Flat Plate," Phys. Scr., **96**(8), p. 085206.
[36] Bollati, J., Semitiel, J., and Tarzia, D. A., 2018, "Heat Balance Integral Methods Applied to the One-Phase Stefan Problem With a Convective Boundary Condition at the Fixed Face," Appl. Math. Computation, **331**, pp. 1–19.
[37] Hayashi, Y., Komori, T., and Katayama, K., 1975, "Analytical and Experimental Investigation of Self-Freezing," ASME J. Heat Mass Transfer-Trans. ASME, **73**(3), pp. 321–325.
[38] Chaurasiya, V., and Singh, J., 2022, "An Analytical Study of Coupled Heat and Mass Transfer Freeze-Drying With Convection in a Porous Half Body: A Moving Boundary Problem," J. Energy Storage, **55**, p. 105394.
[39] Swain, K., Mahanthesh, B., and Mebarek-Oudina, F., 2021, "Heat Transport and Stagnation-Point Flow of Magnetized Nanoliquid With Variable Thermal Conductivity, Brownian Moment, and Thermophoresis Aspects," Heat Transfer, **50**(1), pp. 754–767.
[40] Chaurasiya, V., Rai, K. N., and Singh, J., 2022, "Heat Transfer Analysis for the Solidification of a Binary Eutectic System Under Imposed Movement of the Material," J. Therm. Anal. Calorim., **147**, pp. 3229–3246.
[41] Chaurasiya, V., Rai, K. N., and Singh, J., 2021, "A Study of Solidification on Binary Eutectic System With Moving Phase Change Material," Therm. Sci. Eng. Prog., **25**, p. 101002.
[42] Asogwa, K. K., Mebarek-Oudina, F., and Animasaun, I. L., 2022, "Comparative Investigation of Water-Based al2o3 Nanoparticles Through Water-Based Cuo Nanoparticles Over an Exponentially Accelerated Radiative Riga Plate Surface Via Heat Transport," Arabian J. Sci. Eng., **47**, pp. 8721–8738.
[43] Chaurasiya, V., Kumar, D., Rai, K. N., and Singh, J., 2022, "Heat Transfer Analysis Describing Freezing of a Eutectic System by a Line Heat Sink With Convection Effect in Cylindrical Geometry," Z. Für Naturforsch. A, **77**(6), pp. 589–598.
[44] Chabani, I., Mebarek-Oudina, F., and Ismail, A. A. I., 2022, "Mhd Flow of a Hybrid Nano-Fluid in a Triangular Enclosure With Zigzags and an Elliptic Obstacle," Micromachines, **13**(2), p. 224.
[45] Asogwa, K. K., Goud, B. S., Reddy, Y. D., and Ibe, A. A., 2022, "Suction Effect on the Dynamics of Emhd Casson Nanofluid Over an Induced Stagnation Point Flow of Stretchable Electromagnetic Plate With Radiation and Chemical Reaction," Results Eng., **15**, p. 100518.
[46] Kumar, A., Singh, A., and Rajeev, 2020, "A Moving Boundary Problem With Variable Specific Heat and Thermal Conductivity," J. King Saud Univ.-Sci., **31**(1), pp. 384–389.
[47] Raghavan, G. S. V., Tulasidas, T. N., Sablani, S. S., and Ramaswamy, H. S., 1995, "A Method of Determination of Concentration Dependent Effective Moisture Diffusivity," Drying Technol., **13**, pp. 1477–1488.
[48] Warke, A. S., Ramesh, K., Mebarek-Oudina, F., and Abidi, A., 2022, "Numerical Investigation of the Stagnation Point Flow of Radiative Magneto-micropolar Liquid Past a Heated Porous Stretching Sheet," J. Therm. Anal. Calorim., **147**, pp. 6901–6912.
[49] Hassan, M., Mebarek-Oudina, F., Faisal, A., Ghafar, A., and Ismail, A. I., 2022, "Thermal Energy and Mass Transport of Shear Thinning Fluid Under Effects of Low to High Shear Rate Viscosity," Int. J. Thermofluids, **15**, p. 100176.
[50] Razzaghi, M., and Yousefi, S., 2001, "The Legendre Wavelets Operational Matrix of Integration," Int. J. Syst. Sci., **32**(4), pp. 495–502.
[51] Ray, S. S., and Gupta, A. K., 2017, "Two-Dimensional Legendre Wavelet Method for Travelling Wave Solutions of Time-Fractional Generalized Seventh Order Kdv Equation," Comput. Math. Appl., **73**(6), pp. 1118–1133.
[52] Kumar, D., Upadhyay, S., Singh, S., and Rai, K. N., 2017, "Legendre Wavelet Collocation Solution for System of Linear and Nonlinear Delay Differential Equations," Int. J. Appl. Comput. Math., **3**, pp. 295–310.
[53] Jitendra, Chaurasiya, V., Rai, K. N., and Singh, J., 2022, "Legendre Wavelet Residual Approach for Moving Boundary Problem With Variable Thermal Physical Properties," Int. J. Nonlinear Sci. Numer. Simul., **23**, pp. 957–970.
[54] Upadhyay, S., Kumar, D., Singh, S., and Rai, K. N., 2015, "Numerical Solution of Two Point Boundary Value Problems by Wavelet Galerkin Method," Int. J. Appl. Math. Res., **4**(4), pp. 496–512.
[55] Jain, A., and Parhizi, M., 2021, "Conditionally Exact Closed-Form Solution for Moving Boundary Problems in Heat and Mass Transfer in the Presence of Advection," Int. J. Heat Mass Transfer, **180**, p. 121802.
[56] Chaudhary, R. K., Chaurasiya, V., and Singh, J., 2022, "Numerical Estimation of Temperature Response With Step Heating of a Multi-Layer Skin Under the Generalized Boundary Condition," J. Therm. Biol., **108**, p. 103278.
[57] Chaudhary, R. K., Chaurasiya, V., and Singh, J., 2022, "A Numerical Study on the Thermal Response in Multi-Layer of Skin Tissue Subjected to Heating and Cooling Procedures," Eur. Phys. J. Plus, **137**, p. 120.
[58] Chaudhary, R. K., and Singh, J., 2022, "Numerical Analysis of Thermal Response on a Non-Linear Model of Multi-Layer Skin Under Heating and Cooling Processes," Int. Commun. Heat Mass Transfer, **139**, p. 106467.